Engineering Structures 59 (2014) 484–494

Contents lists available at ScienceDirect

Engineering Structures

journal homepage: www.elsevier.com/locate/engstruct

Modeling of reinforcement global buckling in RC elements

Leonardo M. Massone *, Eduardo E. López

Department of Civil Engineering, University of Chile, Blanco Encalada 2002, Santiago, Chile

ARTICLE INFO

Article history:
Received 17 June 2013
Revised 23 October 2013
Accepted 11 November 2013
Available online 15 December 2013

Keyword:
Buckling
Local
Global
Reinforcement
Reinforced concrete
Columns
Model

ABSTRACT

Buckling of longitudinal reinforcement in reinforced concrete (RC) columns or walls is commonly seen with a length equal to the spacing between stirrups (local buckling), but experimental observations have shown that the length of buckling can span a larger length, deforming several stirrups within the buckling length (global buckling).

The behavior of the longitudinal reinforcement under compression resulting in global buckling is studied in this work, based on a concentrated plasticity fiber model that considers four (4) plastic hinges. The model was originally validated for local buckling and here is extended to global buckling by introducing the effect of transversal reinforcement and expansion of the core concrete in the analysis. Modeling of the forces from the stirrups acting on the longitudinal bar assumes that part of the force is transferred directly to the expanding concrete core and the remaining force is balanced by internal stresses in the longitudinal bar.

The bar buckling behavior is evaluated for different buckling length values and the length is chosen such that it delivers the lowest maximum stress. The proposed model is validated by comparison of the predicted buckling mode with experimental test results from the literature. The average error in the mode prediction is −0.59 (about half the space between stirrups), which is a reasonably good value considering that the database of tests used covers buckling modes from 1 to 7 (stirrup spacing). Besides of providing good critical buckling length predictions, it allows obtaining the stress versus strain curve for the overall buckling bar.

Analysis of three column specimens from the literature indicates that the overall stress versus strain response can be obtained with a reasonable accuracy. Peak stress is obtained within an error of about 10% compared to the test result for a strain well represented by the model. The post-peak slope also gives a good estimate for the degradation stage.

1. Introduction

In a seismic context, elements designed to withstand significant forces and deformations in compression or large tensile strains followed by compression, which could happen in columns or walls boundary elements, should account for potential loss of resistance generated by the buckling of longitudinal reinforcement. It has been observed that the concrete cover, since it is not confined, spalls at longitudinal strain values between 0.003 and 0.004 [1], therefore, does not constitute an effective lateral restraint and buckling of longitudinal reinforcement is avoided or limited by the resistance of the stirrups.

Usually, buckling of longitudinal reinforcement is considered located in a length determined by the distance between stirrups, which is called local buckling of the reinforcement (Fig. 1a). However, experimental observations have shown that in elements with a good distribution of stirrups, the buckling length may be longer, stretching those stirrups that are within the buckling length, prevailing over the local buckling. This is called global buckling of the reinforcement (Fig. 1b). Thus, the buckling length is not completely determined by the spacing of stirrups, but also by the flexibility of the reinforcement (longitudinal and transversal). In order to study this phenomenon it is necessary to appropriately reproduce the behavior of the elements involved in rebar buckling.

The objective of this work is to use an existing model [2], which has shown good performance in representing the local buckling of reinforcing and extending its application to global buckling.

2. Literature review

One of the first works that studied buckling of longitudinal reinforcement in concrete columns is the publication by Bresler and Gilbert [3]. Among its contributions are a method that predicts the critical load and buckling shape providing the minimum stiffness (or minimum diameter) of the stirrups in order to limit their elongation while the longitudinal reinforcement deforms, and therefore, avoiding global buckling.

* Corresponding author. Tel.: +56 229784984.
E-mail address: lmassone@ing.uchile.cl (L.M. Massone).

0141-0296/$ - see front matter © 2013 Elsevier Ltd. All rights reserved.
http://dx.doi.org/10.1016/j.engstruct.2013.11.015

Nomenclature

A_i	tributary area of each fiber i
A_t	sectional area of a stirrup bar
d_b	diameter of longitudinal reinforcement
d_t	diameter of transverse reinforcement
e	imperfection applied at the bar mid-length, set as $e = 0.01 d_b$ to avoid obtaining the solution without buckling effect (trivial solution)
EI	reduced stiffness (a section going in compression within the hardening region of steel and another going under elastic unloading).
E_0	initial elastic reloading/unloading module, set as $E_0 = E_s(1 - \Delta\varepsilon)$ [7].
E_c	concrete elastic modulus
E_s	steel stiffness
E_t	stirrups bar elastic modulus
f'_c	unconfined compressive strength of concrete
F_j	stirrups total forces
F_j^h	stirrups forces due to the concrete expansion
k	longitudinal reinforcement normalized stiffness
k_{eq}	equivalent stiffness (normalized)
k_t	stirrup stiffness
k_v	calibration factor for ε_{ct}
l_p	plastic hinge length, set as $l_p = d_b$
l_t	stirrup total length
l'_t	stirrup effective length
$L_{mode\ i}$	buckling length of mode i, set as $L_{mode\ i} = i \cdot s$
L	buckling bar length
m	internal hinge moment, set as $m = \sum_i \sigma_i A_i x_i$
M	internal hinge moment for global buckling
n_l	number of reinforcing bars subjected to buckling in the direction of analysis
n_t	number of stirrups in the considered direction
N	number of stirrups within the buckling length
N'	number of stirrups for analysis
p	applied load, set as $p = -\sum_i \sigma_i A_i$
P	applied load for global buckling
P_c	critical load
P_o	critical load for a buckling length of s
Q	curve A parameter, set as $Q = ((\sigma_f - \sigma_0)/(\varepsilon_f - \varepsilon_0)E_0 - a)/(1 - a)$, with $a = (1 + (E_0(\varepsilon_f - \varepsilon_0)/(\sigma_f - \sigma_0))^R)^{-1/R}$
R	parameter representing the Bauschinger effect, set as $R = 14(\varepsilon_y)^{1/3}(1 - 14\Delta\varepsilon)$ for the unloading stage and $R = 20(\varepsilon_y)^{1/3}(1 - 18\Delta\varepsilon)$ for the reloading stage [7].
s	spacing of stirrups
v	vertical displacement
w	Additional lateral deformation associated to a vertical displacement v
x_i	location of fiber i
x_j	vertical distance of the force ΔF_j relative to the extreme hinge
x_j^0	vertical distance x_j at the beginning of the analysis
y_j	transverse displacement of the force ΔF_j
α	function of the steel stiffness and the stirrups arrangement
γ	stiffness parameter
ΔF_j	stirrups forces associated to longitudinal reinforcement buckling, set as $\Delta F_j = F_j - F_j^h$
$\Delta\varepsilon$	half cyclic strain variation, set as $\Delta\varepsilon = \lvert\varepsilon_f - \varepsilon_0\rvert/2$.
ε	axial strain at mid-section
$\bar{\varepsilon}$	resultant average bar strain
ε_o	strain at the beginning of curve A
ε_{uc}	strain at unconfined compressive strength of concrete
ε_{cc}	confined concrete compressive strain at the maximum stress, set as $\varepsilon_{cc} = \varepsilon_{uc}\left(1 + \frac{24.6 k_e \rho_s \sigma_y}{f'_c}\right)$
ε_{ct}	strains in the stirrups due to the lateral expansion of the concrete core
ε_f	strain at the end of curve A
ε_i	axial strain at location x_i, set as $\varepsilon_i = \varepsilon + \phi x_i$ (Bernoulli hypothesis)
ε_m	peak strain
ε_{sh}	strain at initiation of strain hardening
ε_{wj}	strains in the stirrups due to longitudinal reinforcement buckling
ε_y	yield strain
θ	hinge rotation, set as $\theta = \phi \cdot l_p$
θ_e	initial rotation due to imperfection e, set as $\theta_e = \tan^{-1}(e/(L/2 - l_p))$
θ_p	rotation due to lateral displacement w
ϕ	curvature
ν_o	concrete Poisson's modulus
ρ_s	amount of volumetric transverse reinforcement
$\bar{\sigma}$	resultant average bar stress
σ_i	steel stress at location x_i
σ_0	stress at the beginning of curve A
σ_f	stress at the end of curve A
σ_m	peak stress
σ_y	yield stress

Scribner [4] focused the attention in reproducing the observed behavior of beams during bending tests, noting that buckling of the longitudinal reinforcement typically occurs where the concrete has spalled, which corresponds approximately to a length of the height of the beam. Scribner models buckling over a length equal to three stirrup spacing. Similar to the work by Bresler and Gilbert, the critical load is estimated. Based on an energy model of the system, a simplified expression is analytically determined to limit the diameter of the bars to promote a local buckling failure over a global buckling failure, suggesting that the ratio of the diameter of longitudinal reinforcement (d_b) to the transverse reinforcement (d_t) should be $d_b/d_t = 1.85$. Performing a similar analysis, the diameter ratio for a buckling length of two stirrup spacings is 1.69, and considering a buckling length of four spacings is 2.11.

According to Papia et al. [1] in many tests of strongly confined concrete columns it has been observed that buckling of longitudinal reinforcing involves deforming stirrups, and causing them to fail in tension. The loss of confinement accelerates failure of the column, being able to reach a lower strain level than expected with full confinement. Once concrete cover spalls, the longitudinal bar is free to deform outward. When reaching the critical buckling conditions for the longitudinal bar, and the column has a suitable confinement, the longitudinal reinforcement is commonly in the region of strain hardening and the transverse reinforcement could be either in the linear-elastic or strain hardening zone, depending on the transversal strain.

They proposed a model that assumes a positive symmetrical shape function representing the transversal deformation of the longitudinal bar, and based on the system energy, the critical condition is established. Based on their methodology, the critical load ratio (P_c/P_o) and critical buckling length (L/s) are provided, which is dependent on $\gamma = \frac{\alpha s^3}{EI}$, where L is the buckling bar length, s is the spacing of stirrups, α, is a function of the steel stiffness and the stirrups arrangement, P_c is the critical load of the problem analyzed, $P_0 = \frac{\pi^2 EI}{s^2}$ the critical load for a buckling length of s with the same

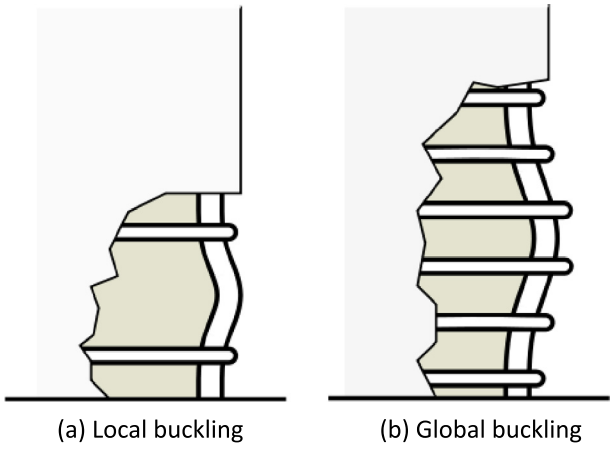

Fig. 1. Longitudinal reinforcement buckling mode – (a) Local buckling, and (b) Global buckling.

material properties, and EI is a reduced stiffness based on part of the cross-section going in compression within the hardening region of steel and another part of the cross-section going under elastic unloading.

Thus, they constructed the curve $C_c = P_c/P_o$ in Fig. 2, which relates the stiffness parameter γ of the stirrups, with the critical buckling load and the length of the bar. Additionally, the curve L/s is included [5], which is related to the number of stirrups within the buckling length. Calculation of parameter γ requires the value of the stirrups stiffness, α, which depend on the configuration of stirrups and the steel stiffness (E_s) at the buckling condition (linear-elastic zone or hardening). Different configurations are considered for longitudinal and transverse reinforcement, which for a corner longitudinal bar, results in $\alpha = 2\frac{E_s A_t}{l_t}$ (other cases are similar), with A_t sectional area of a stirrup bar and l_t the stirrup length.

Dhakal and Maekawa [6], similarly to other authors, determined the critical load based on the energy stored in the system by equating and matching the energy for 2 consecutive failure modes. The model assumes a sinusoidal deformed shape within the buckling length with the stirrups simulated as discrete elastic springs whose rigidity is zero, if they are located within a central section of the buckled length and elastic elsewhere. The flexural rigidity of the longitudinal bar is simplified and explicitly determined considering that it is beyond the elastic region, as $EI = 0.5E_sI\sqrt{\frac{\sigma_y}{400\ \text{MPa}}}$, where E_s is stiffness of the elastic section, σ_y is the yield stress. The longitudinal reinforcement normalized stiffness is defined as $k = \frac{\pi^4 EI}{s^3}$. The stirrup stiffness, $k_t = \frac{E_t A_t}{l_t'}\frac{n_t}{n_l}$, is calculated as the axial stiffness of one stirrup multiplied by the number of stirrups in the considered direction, n_t (Fig. 3), divided by the number of reinforcing bars subjected to buckling in the direction of analysis, n_l (Fig. 3), where E_t is the stirrups bar elastic modulus and l_t' is the stirrup effective length. The equivalent stiffness (normalized) limit values, $k_{eq} = k_t/k$, for the different buckling modes are tabulated in Table 1.

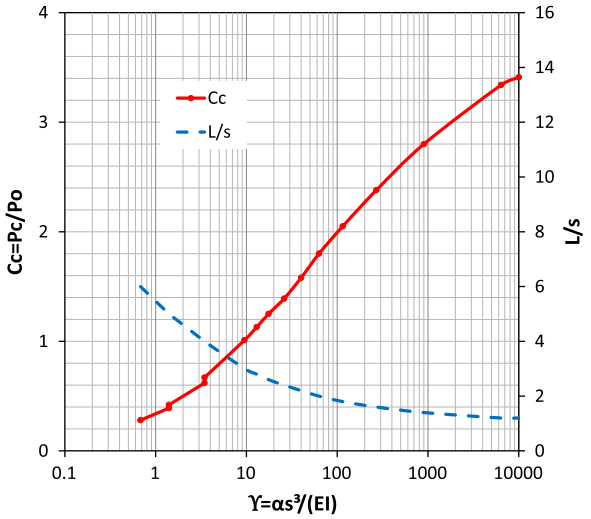

Fig. 2. Critical load and buckling length (after [1,5]).

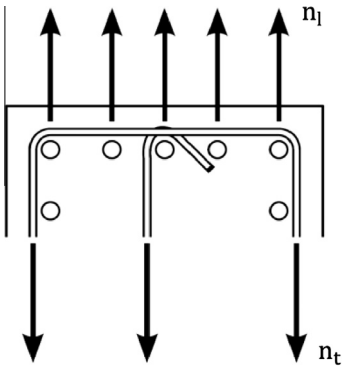

Fig. 3. Buckling scheme of a group bar.

Table 1
k_{eq} Values for different buckling modes (after [6]).

Buckling mode, n	k_{eq} avg
1	0.7500
2	0.1649
3	0.0976
4	0.0448
5	0.0084
6	0.0063
7	0.0037
8	0.0031
9	0.0013
10	0.0009

All previous models were intended to determine the critical load and the number of stirrups involved. The model described in this study, besides of predicting the buckling mode, provides the stress–strain curve for the buckled bars (σ–ε) which can be used in sectional, element or system nonlinear analysis. Current design in many cases (e.g., in tall buildings in Los Angeles, California) involve nonlinear analysis often within the performance-based design framework. It would be even more beneficial for assessment of existing buildings, since in those cases provisions for transversal reinforcement diameter from current design codes that intend to prevent global buckling of reinforcement might not be present.

3. Concentrated plasticity model – local buckling

The model described by Massone and Moroder [2] is used to study the buckling response of bare longitudinal reinforcement, which captures the behavior of reinforcement in monotonic compression without constrains in its length, and has been slightly modified by Lacaze [7]. The original model considers a bar with fixed ends free to move vertically in its upper end, with an initial imperfection given by a lateral displacement in the middle of its length. The deformations are concentrated in four plastic hinges located symmetrically at positions of maximum moment for a point load or imperfection e applied at the bar mid-length (Fig. 4). Additional lateral deformation w is associated to a vertical displacement v of the free end due to an applied load p. The plastic hinge length is set as the bar diameter, $l_p = d_p$, with a constant curvature

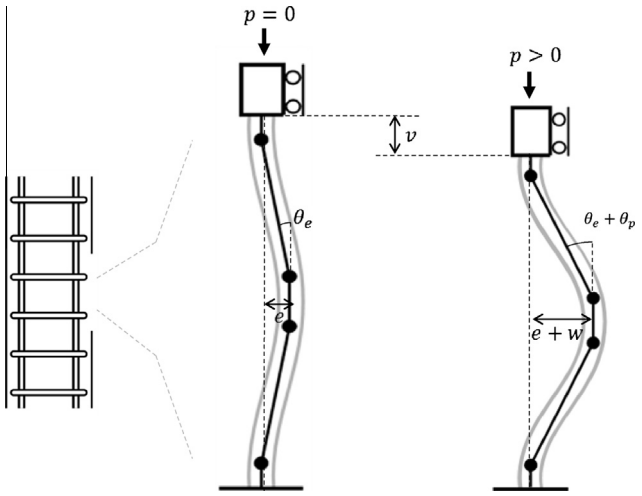

Fig. 4. Local buckling model with initial imperfection (after [2]).

distribution along it, such that the hinge rotation, θ, is related to the curvature ϕ. The imperfection e can be introduced as an initial rotation θ_e.

At the beginning of the axial loading, the load p and the moment m at the hinges are zero. A vertical displacement v of the upper end has an associated additional rotation of the hinge θ_p and a lateral displacement of the central zone of the bar w. The relationship between rotation and lateral movement is given by,

$$e + w = (L/2 - l_p)\sin(\theta_e + \theta_p)/\cos\theta_e \tag{1}$$

Lacaze [7] introduces a change in the original model in order to represent cyclic behavior and properly characterize the response in tension without hinge formation. For this purpose, rotations (curvatures) are concentrated at the plastic hinge, but axial deformations are distributed along the bar.

The internal forces at the hinges are determined by the axial strain at mid-section, ε, and the curvature, ϕ. The cross-section is discretized into a finite number of axially deformable fibers (i.e., 20 fibers), with each fiber having a strain ε_i. By means of the constitutive material law, the steel stress is obtained for each fiber i (σ_i) of tributary area A_i, resulting, by equilibrium, in an axial force p and a moment m at the hinge.

The resultant average bar stress ($\bar{\sigma}$) and strain ($\bar{\varepsilon}$) are,

$$\bar{\sigma} = \frac{p}{\sum_i A_i} \tag{2}$$

$$\bar{\varepsilon} = \frac{v}{L} = \varepsilon + \left(1 - 2\frac{l_p}{L}\right)\left[1 - \frac{\cos(\theta_e + \theta_p)}{\cos\theta_e}\right] \tag{3}$$

The numerical nonlinear problem is reduced to a 1 DOF system, where given an axial deformation, $\bar{\varepsilon}$, the formulation iterates over the value for the additional curvature, ϕ_p, until equilibrium defined as Eq. (4) is achieved (within a tolerance). Equilibrium is determined for a quarter of the bar, such that it involves an inflexion point (zero moment) and another end within the plastic hinge with moment m, with a relative lateral displacement of $(e + w)/2$.

$$m = p(e + w)/2 \tag{4}$$

The currently implemented model considers that the initial imperfection is present in the bar without residual stresses, i.e., the bar was not deformed, but intrinsically has an imperfection.

3.1. Monotonic steel model

Tensile response is modeled as suggested by Mander et al. [8]. The model considers an elasto-plastic behavior with initial stiffness E_s, and a yield stress and strain point given by $(\sigma_y, \varepsilon_y)$. Strain hardening starts from an strain value of ε_{sh} and ends at the point $(\varepsilon_m, \sigma_m)$ where the peak stress is reached. A linear degradation is defined from the peak stress point to fracture.

Commonly, steel compression behavior is represented by the same curve as for the steel in tension. However, the use of engineering coordinates (referred to initial length and cross-section) gives no reliable values due to important variation of the reinforcement cross-section and length at large drift values. The use of true coordinates, adopted in this work, allows considering the fact that the area changes as the load is applied. The response in compression taken as identical to tension in true coordinates provides a good correlation until reaching the buckling load [9].

3.2. Cyclic steel model

The steel cyclic model is based on a simple phenomenological formulation that requires unloading and reloading rules. In principle, the curves for the tensile and compressive monotonic steel are maintained, but outside the linear range the unloading point continues towards a point (end) with the same strain as in the previous reloading point, according to curve A (Fig. 5), which represents the Bauschinger effect. Curve A can be used as a transition point between unloading/reloading points, which has the form,

$$\sigma_s = \sigma_0 + E_0(\varepsilon_s - \varepsilon_0)\left(Q + (1 - Q)\Big/\left(1 + \left(E_o\left(\frac{\varepsilon_s - \varepsilon_0}{\sigma_f - \sigma_0}\right)\right)^R\right)^{1/R}\right) \tag{5}$$

where R is the parameter representing the Bauschinger effect (the smaller the value of R, the smoother the transition), E_0 is the initial elastic reloading/unloading module, ε_0 and σ_0 are strain and stress at the beginning of curve A, and ε_f and σ_f are the strain and stress at the end of curve A. Q is a shape parameter. The values of E_0 and R suggested by Lacaze [7] provide good cyclic predictions of the model.

The implementation for the first cycle involves knowing the end point of curve A, which was obtained originally by first shifting the steel envelope stress–strain curve to a point where elastic unloading results in zero stress, and then estimating the stress in the shifted curve at zero strain. However, Lacaze compared results obtained with this modeling approach and test results for the first cycle, and improved the response by taking the final point strain value equal (absolute) to the maximum attained in the opposite direction. For subsequent cycles the start and end points correspond to points (strains) at the previous unloading and reloading

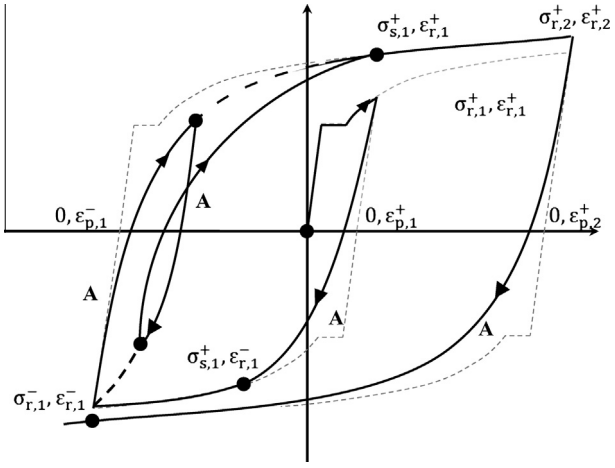

Fig. 5. Cyclic material model (after [2,7]).

points. After reaching the end of curve A, it returns to the shifted monotonic envelope. For internal cycles the end point corresponds to the start of the outer loop, rather than the inside loop (Fig. 5).

The need of a cyclic material lays in the fact that under monotonic compression of a bar and before instability clearly affects the response, all fibers are under compression. At larger compressive strains and considering that instability results in buckling the most compressive fiber goes further in compression (inside of concave zone of buckling), whereas other fibers towards the other end of the section would revert the strain direction resulting in unloading. In the case of cyclic analysis with buckling the entire material cyclic definition is required.

4. Concentrated plasticity model – global buckling

Global buckling is introduced in the model (local buckling) for concentrated plasticity by Massone and Moroder [2], and modified by Lacaze [7]. Global buckling incorporates the effect of stirrups along the buckled shape of the longitudinal reinforcement, as well as the impact of concrete expansion. Thus, overall response of longitudinal reinforcement in columns or wall boundary elements can be studied with the formulation.

The buckling length, L, is associated to discrete buckling modes, where an index i is used to identify how many spaces between stirrups cover the buckled shape of the longitudinal bar. Thus, *mode i* correspond to a buckling length $L_{mode\ i} = i \cdot s$, with s the distance between stirrups, so that local buckling of reinforcement is represented by *mode* 1, and, in general, the total number of stirrups considered for the analysis is given by $N = i + 1$. For modes $i > 1$, the model requires, considering that at early stages of compressive strains concrete cover spalls, that the constraining effect from the stirrups is incorporated.

Previous researches have considered (e.g. [1,10]) that the lateral expansion of concrete is enough to cause the stirrups large strains, such that they are in the hardening region of the steel stress–strain response once buckling of longitudinal reinforcement occurs. On the other hand, Dhakal and Maekawa [6] mentioned that this expansion is not enough to take the stirrup beyond the elastic range; however, their model approach considered that the expansion of concrete consumes almost all the elastic deformation of the steel. Thus, the concrete presence should not be neglected. In fact, ignoring the concrete expansion effect practically leads to only local buckling, that is, between 2 consecutive stirrups, given their high stiffness and strength. Thus, for stirrups within the buckling length of the longitudinal reinforcement, two sources of deformation are considered: first, the lateral expansion undergone by the confined concrete, and second, the additional tensile strain by lateral displacement of the longitudinal bar once buckling starts.

The bar that is susceptible of buckling is initially in contact with the concrete core, but once buckling starts lateral confinement is reduced facilitating the expansion of the concrete inside the buckled length of the bar, so that, contact between reinforcement and concrete can be maintained. Thus, the forces are transmitted from the stirrups to the concrete core, as well as to internal stresses in the longitudinal bar. In order to introduce the force in the stirrups, initially, an intermediate stage would be considered, where for an axial imposed strain, $\bar{\varepsilon}$, the bar does not buckle, Fig. 6b, and strains in the stirrups are only due to the lateral expansion of the concrete core, ε_{ct}, considered identical for all stirrups. Under these conditions, the stirrups forces only due to the concrete expansion, F_j^h, are transmitted completely to the concrete core.

When considering the longitudinal reinforcement buckling an additional strain is introduced into each stirrup, ε_{wj}, which is associated to a force increment, ΔF_j, as shown in Fig. 6c. These additional forces are balanced by internal moments at the hinges, regardless of an increase in the concrete core within the buckled bar length. The internal moment of a hinge, M, is identical for all hinges, because they share the same rotation, balancing the additional forces in the stirrups, ΔF_j, and the moment generated by the eccentricity of the axial force, $P \cdot (e + w)$. Then, the analysis is reduced to capture the effect of incremental forces on the bar, and given the symmetry only half of the total bar length is considered, as shown in Fig. 7. Thus, the problem considers the stirrups 1 to N', where N' depends on whether N (number of stirrups within the buckled bar length) is even ($N' = N/2$, see Fig. 7a) or odd ($N' = (N + 1)/2$, see Fig. 7b), where in the case of an odd value of N, half of the force $F_{N'}^h$ should be considered. It is considered that the forces ΔF_j act perpendicularly to the main direction of reinforcement, i.e., the stirrups only work in tension, neglecting other actions. Then the equilibrium equation for the hinges in the middle of the bar is given by Eq. (6), where x_j is the vertical distance of the force ΔF_j relative to the extreme hinge, which in the case of Fig. 7 corresponds to the upper hinge.

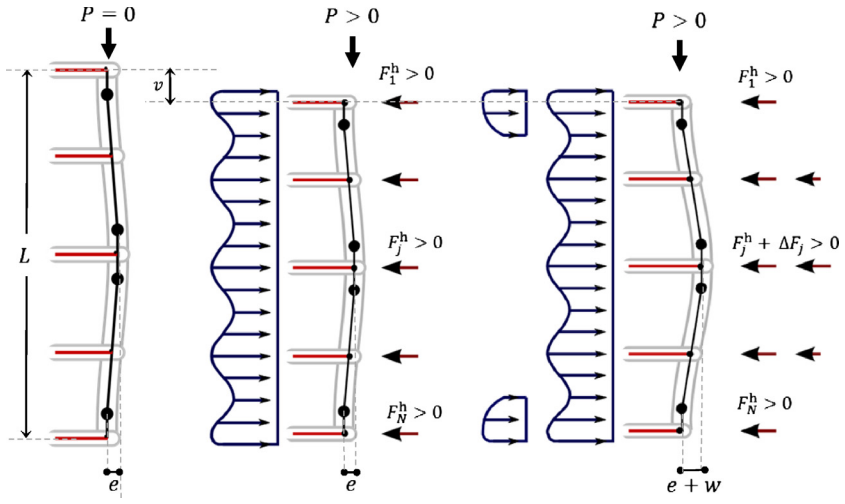

(a) Initial condition (b) Deformed state without buckling (c) Deformed state with buckling

Fig. 6. Global buckling model scheme – (a) Initial condition, (b) Deformed state without buckling, and (c) Deformed state with buckling.

$$P \cdot (e + w) + \sum_{j=2}^{N\prime} \Delta F_j \cdot x_j - 2 \cdot M = 0 \tag{6}$$

When the upper end moves the bar sections incline, then the distance x_j varies as displacement of the upper end, v, increases. It is assumed that the stirrup does not slide with respect to the longitudinal bar and therefore the force exerted by each stirrup is firmly joined to a fixed point of the model. Thus, x_j depends on the section of the bar where the stirrup is located. If x_j^0 is called the x_j distance at the beginning of the analysis, at any other instant x_j is given by Eq. (7). For small deformations it can be assumed that $x_j = x_j^0$.

$$x_j = \begin{cases} x_j^0 \cdot \frac{\cos(\theta_e+\theta_p)}{\cos(\theta_e)} & \text{if} \quad 0 < x_j^0 < \frac{L}{2} - \frac{l_p}{2} \\ x_j^0 + \left(\frac{L}{2} - l_p\right)\left(\frac{\cos(\theta_e+\theta_p)}{\cos(\theta_e)} - 1\right) & \text{if} \quad \frac{L}{2} - \frac{l_p}{2} \le x_j^0 \end{cases} \tag{7}$$

Similarly, the transverse displacement (y_j) due to buckling also depends on the zone of the longitudinal bar where the stirrup is located, as shown in Eq. (8). This displacement is added to the initial imperfection e and it is related to the strain imposed to the stirrup. In Eqs. (7) and (8), L is the initial length of the bar, θ_e and θ_p are rotations due to the initial imperfection e and the additional displacement w described in the original model (local buckling) and l_p corresponds to the plastic hinge length. Fig. 8 presents a scheme of x_j, x_j^0 and y_i., which helps understanding the formulation of Eqs. (7) and (8). In the figure, the stirrups are considered that they do not slide over the longitudinal bar and the portion of the longitudinal bar between hinges does not shorten for simplification. This implies that x_j and x_j^0 share a common side along the longitudinal bar. Similarly, assuming that common shared side along the bar helps determining the additional transversal deformation from stirrups (beyond the imperfection) y_j.

$$y_j = \begin{cases} x_j^0 \cdot \frac{\sin(\theta_e+\theta_p)}{\cos(\theta_e)} - x_j^0 \cdot tan(\theta_e) & \text{if} \quad 0 < x_j^0 < \frac{L}{2} - \frac{l_p}{2} \\ \left(\frac{L}{2} - l_p\right)\frac{\sin(\theta_e+\theta_p)}{\cos(\theta_e)} - \left(\frac{L}{2} - l_p\right)tan(\theta_e) & \text{if} \quad \frac{L}{2} - \frac{l_p}{2} \leqslant x_j^0 \end{cases} \tag{8}$$

4.1. Forces in stirrups and cross-ties

As stated earlier, in order to correctly characterize the response of stirrups and cross-ties the concrete core expansion, as well as

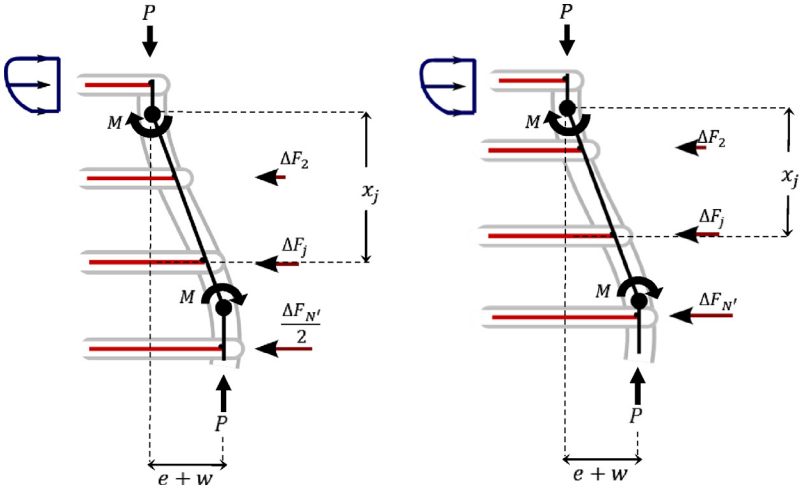

Fig. 7. Free body diagram of global buckling (half bar) – (a) Even N value, and (b) Odd N value.

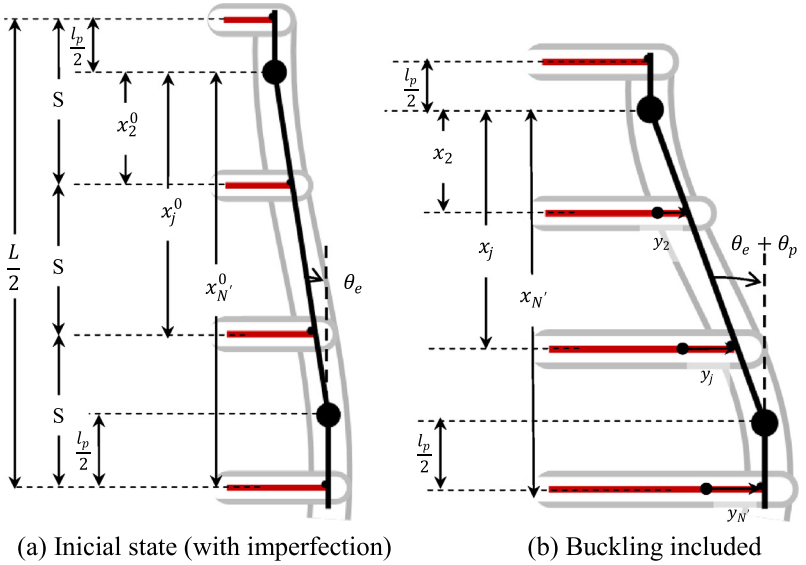

Fig. 8. Location of transversal reinforcement (x_j) and deformation (y_j) – (a) Initial state (with imperfection), and (b) buckling included.

the additional deformation that comes from the buckled bar should be considered. The total force on each stirrup, F_j, is determined by the total strain, which considers both the deformation due to the concrete lateral expansion, ε_{ct}, and the lateral deformation that imposes the buckled bar, ε_{wj}. Two steel models are considered to characterize the steel response of stirrups to better capture the available experimental data [8,11]. In both cases, after reaching the maximum stress, the capacity remains constant.

The force ΔF_j corresponds to the additional force above the one introduced by concrete expansion, F_j^h, which is described as $\Delta F_j = F_j - F_j^h$, as shown in Fig. 9.

4.1.1. Concrete core expansion, ε_{ct}

The strain ε_{ct} is dependent of the concrete axial strain, which in this case is taken as the average axial strain $\bar{\varepsilon}$ within the buckling length. This strain can be determined with the Eq. (9) for any average axial strain $\bar{\varepsilon}$ [10],

$$\varepsilon_{ct} = -v_0\bar{\varepsilon} + (1-2v_0)\frac{k_e\rho_s\sigma_y}{E_c} - \varepsilon_{cc}\frac{(1-2v_0)}{2}\left(\frac{\bar{\varepsilon} - 0.00015/v_0}{\varepsilon_{cc} - 0.00015/v_0}\right)^2 \quad (9)$$

where ε_{cc} is the confined concrete compressive strain at the maximum stress, ρ_s is the amount of volumetric transverse reinforcement, E_c is the concrete elastic modulus, f'_c is the unconfined compressive strength of concrete and ε_{uc} the correspondent strain, v_0 corresponds to the initial Poisson's ratio, which is taken as 0.2 [1,10]. The effectiveness factor of confinement k_e is determined as in Mander et al. [12]. This equation is based on the behavior of concrete with a constant lateral pressure, yielding to uniform strain distribution without showing the reduction of strain expected at the stirrup location.In order to represent the impact of stirrups in the local expansion at their location, a calibration factor k_v is introduced by weighting the volumetric expansion component of the original expression. Besides, for simplicity, the term associated directly to confinement (small contribution) is removed given that confinement is already taking into account. Thus, the expression reduces to,

$$\varepsilon_{ct} = -v_0\bar{\varepsilon} - k_v\varepsilon_{cc}\frac{(1-2v_0)}{2}\left(\frac{\bar{\varepsilon} - 0.00015/v_0}{\varepsilon_{cc} - 0.00015/v_0}\right)^2 \quad (10)$$

Factor k_v that multiplies the volumetric expansion component of Eq. (10) is calibrated according to experimental measurements to adjust the measured strains in stirrups. For this purpose, the data presented by Bayrak and Sheikh [13] for tests carried out elsewhere [14] is used. Least squares method is used to calibrate k_v to the data obtained experimentally as shown in Fig. 10. As an example, specimen 4A3-7 shows the best correlation with $k_v = 0.3$ (Fig. 10b). All other specimens show a similar response, with an average best fit parameter of $k_v = 0.33$ (Fig. 10a), which is used for further analysis.

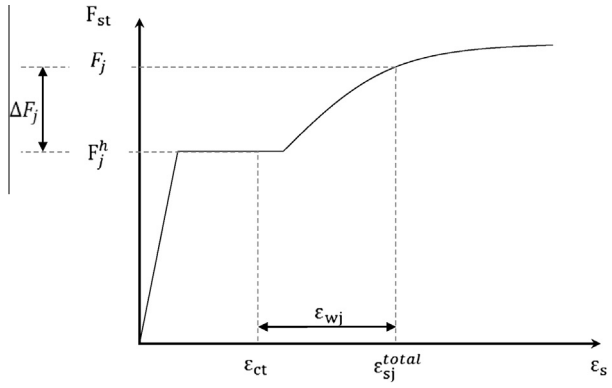

Fig. 9. Force distribution in stirrups.

4.1.2. Stirrup strain due to longitudinal bar buckling, ε_{wj}

Strains or stresses in stirrups are considered, in part, as a resultant from the displacements induced by bar buckling, acting in each contact point in the opposite direction to buckling (outward). Wall boundary elements with little or no confinement would usually result in buckling of the longitudinal reinforcement moving away from the wall face for both layers of reinforcement [15,16]. The same behavior would be expected in columns under pure axial load (Fig. 11). In the case of columns under axial load and bending, it is more probable to have buckling in the most compressed zone. Corner bars are considered to buckle in the main direction, which coincide with the lower stirrup stiffness. Thus, the stirrup strain is given by,

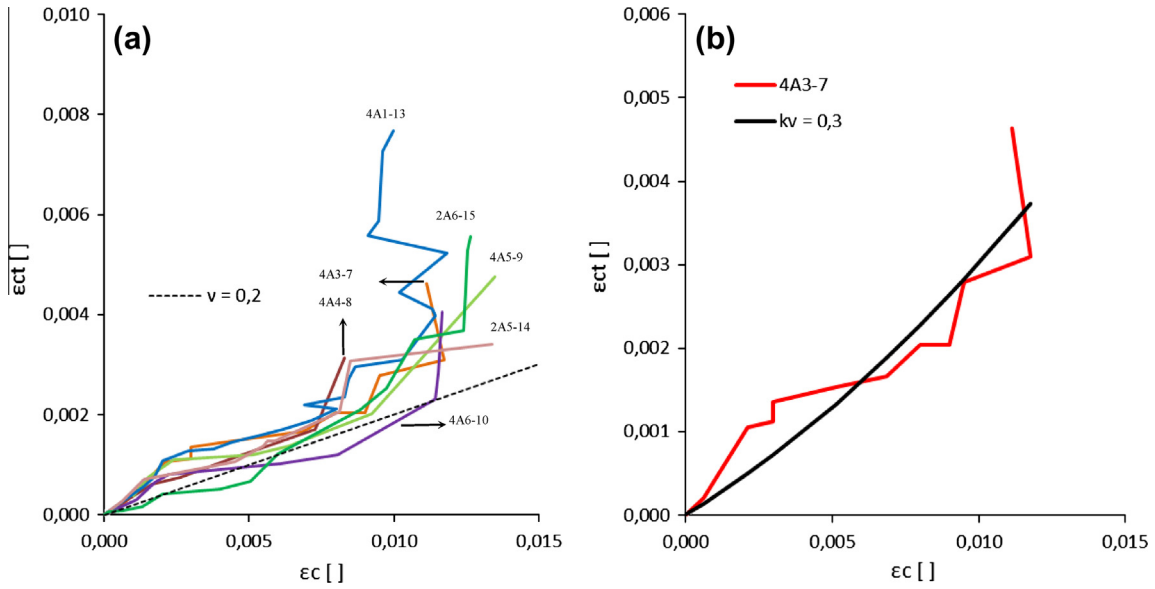

Fig. 10. Calibration of k_v. Experimental data reported by Bayrak and Sheikh [13] – (a) All considered test, and (b) calibration of specimen 4A3-7.

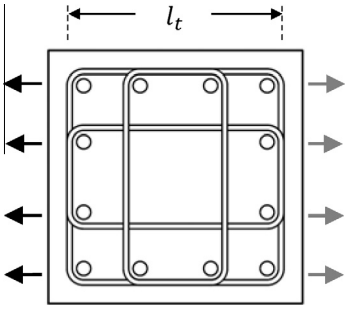

Fig. 11. Direction of buckling.

$$\varepsilon_{wj} = y_j / l'_t \tag{11}$$

where l'_t is the effective length of the stirrup, which can be regarded as the total length (l_t) or half the length ($l_t/2$) depending if the column is in bending or under pure axial compression, respectively. In case of pure axial compression, it is supposed that there is simultaneity and symmetry of buckling (2 opposite sides of the column), such that each longitudinal reinforcement bar acts on a length equal to half the total length of the stirrup. In case of bending, the bars buckle in the region of highest compression of the element section (one side only of the column), acting over the total length of the stirrup, as the bars of the other end being in tension or lower level of compression will not suffer buckling.

4.2. Methodology – buckling of group bars

The analysis of elements such as walls or columns with longitudinal reinforcement prone to buckle, requires defining the number bars that might buckle on one side of the section (n_1), and the number of legs of stirrups providing support against buckling in that direction (n_t), as shown in Fig. 3. The original equilibrium equation (Eq. (6)) for bare bar under global buckling is modified to account for all reinforcement involved in group bar global buckling (longitudinal bars and stirrups) by weighting the corresponding forces (or moment) by n_l and n_t, depending on whether they correspond to longitudinal or transverse reinforcement, respectively, similarly as used by Dhakal and Maekawa [6], yielding:

$$n_l \cdot P \cdot (e + w) + n_t \cdot \sum_{j=2}^{N'} \Delta F_j \cdot x_j - n_l \cdot 2 \cdot M = 0 \tag{12}$$

This methodology attempts to capture an average behavior of all bars, rather than an individual behavior, so that it makes no distinction between bars directly constrained by a stirrup bar or an intermediate bar.

4.2.1. Critical buckling length selection

The analysis considers a known buckling length, L, however, in reality this length depends on the characteristics of the longitudinal reinforcement and the restriction presented by the stirrups to buckling. Thus, the buckling length can cover from one spacing between stirrups (local buckling), s, to a length where several stirrups are involved ($L/s > 1$). It is common to find local buckling when there is a very high axial stiffness of the stirrups compared with the flexural stiffness of the longitudinal reinforcement, as is the case of very thick stirrups or very slender longitudinal reinforcement because of a large separation of stirrups or a small longitudinal reinforcement diameter.

As a selection criterion, it is considered that the buckling mode that yields the lowest peak capacity is the most probably mode, which corresponds to a simple condition consistent with the criterion used by other researchers to estimate the critical buckling load (e.g., [1,6,10]). Due to the shape of the overall stress–strain curves there are two types of behavior: the most common is that the maximum is at a value higher than the yield stress (e.g., Fig. 12a, $L/s = 3$ selected) and another where the differentiation of the curves occurs soon after a drop past yielding (e.g., Fig. 12b, $L/s = 4$ selected), in which case the second peak is considered for the analysis. This is because the major transverse displacement caused by buckling occurs after exceeding the first maximum. Although, this methodology requires this additional effort, its rewards lies in the fact that the stress–strain curve can also be obtained and could be used to model wall or column response.

Analyzing the behavior of the bar for several buckling modes ($L/s = 1, 2, 3$, etc.), in some configurations, might involve analyzing the buckling of a bar with slenderness (L/d_b) less than 4 due to the relatively short distance between stirrups. The original model considers that the plastic hinge length is the diameter of the reinforcement (d_b). Thus, to avoid the overlap of the 4 plastic hinges, their length is limited to $L/4$.

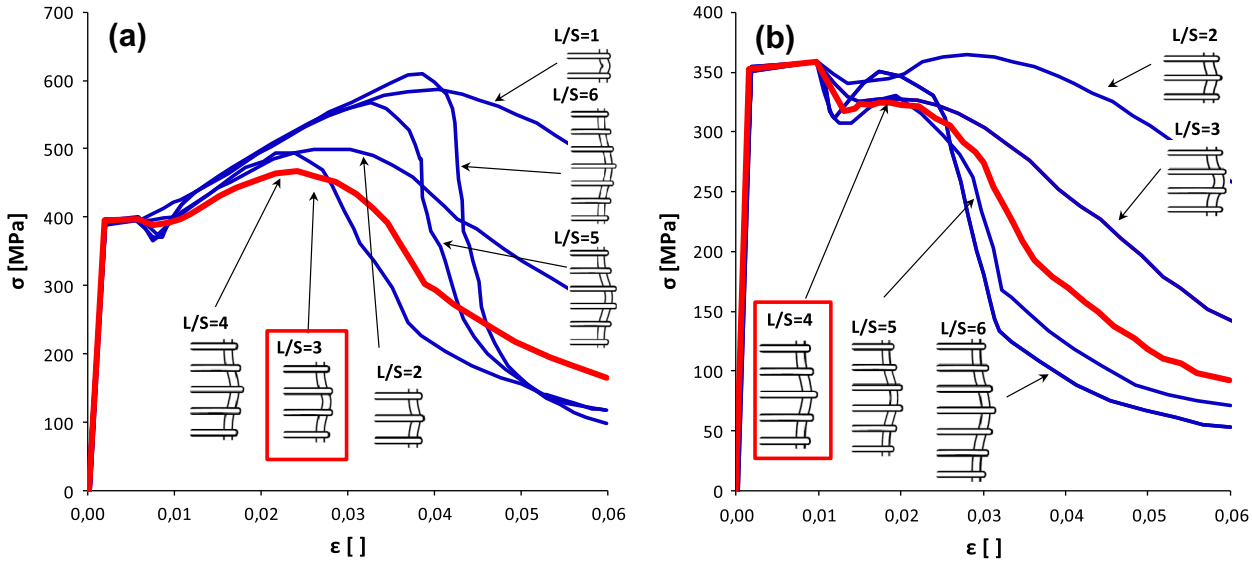

Fig. 12. Critical buckling length selection – (a) minimum peak capacity (most cases), and (b) minimum peak post-yield capacity.

Table 2
Main test parameters and model predictions.

Autor	ID	Long. Reinf.			Transv.	Reinf.	Concrete	L/S		
		n_l	σ_y (MPa)	σ_m (MPa)	n_t	σ_y (MPa)	f'_c (MPa)	Test	D&M	Model
Kato et al. [17] Series A	4D16D10S93	2	342	497	2	352	28	1	1	1
	4D13D10S93	2	343	495	2	352	28	1	1	1
	4D10D10S93	2	379	523	2	352	28	1	1	1
	4D16D6S70	2	342	497	2	348	24.9	3	2	2
	4D13D6S70	2	343	495	2	348	24.9	2	2	2
	4D10D6S70	2	379	523	2	348	24.9	1	1	1
	4D16D6S47	2	342	497	2	348	24.6	4	4	3
	4D13D6S47	2	343	495	2	348	24.6	3	2	2
	4D10D6S47	2	379	523	2	348	24.6	3	2	1
	4D16D6S35	2	342	497	2	348	23.9	5	5	3
	4D13D6S35	2	343	495	2	348	23.9	4	4	3
	4D10D6S35	2	379	523	2	348	23.9	2	2	2
	4D16D4S47	2	342	497	2	583	25.5	5	5	4
	4D13D4S47	2	343	495	2	583	25.5	4	4	4
	4D10D4S47	2	379	523	2	583	25.5	3	2	2
	4D16D4S35	2	342	497	2	583	25.1	6	5	5
	4D13D4S35	2	343	495	2	583	25.1	5	5	5
	4D10D4S35	2	379	523	2	583	25.1	3	3	3
	4D16D4S23	2	342	497	2	583	22	7	7	8
	4D13D4S23	2	343	495	2	583	22	5	5	5
	4D10D4S23	2	379	523	2	583	22	3	5	5
Kato et al. [17] Series B	4D16HD10S140	2	739	847	2	352	64	1	1	1
	4D16LD6S70	2	343	497	2	761	66	2	2	3
	4D13LD6S70	2	336	482	2	761	66	2	2	2
	4D13LD6S47	2	336	482	2	761	64	3	2	3
	4D16HD6S35	2	739	847	2	761	66	4	5	3
	4D16LD6S35	2	343	497	2	761	66	4	5	4
	4D13LD6S35	2	336	482	2	761	66	3	4	3
	4D10LD6S35	2	379	523	2	761	66	2	2	3
(b)										
Ooya and Kato [20]	12D10D6S70	4	351	479	2	363	27.1	1	1*	1
	12D10D6S70I	4	351	479	4	363	27.1	1	1*	1
	12D13D6S47	4	336	482	2	363	27.5	4	4*	3
	12D13D6S47I	4	336	482	4	363	27.5	4	3*	3
	12D10D6S47	4	351	479	2	363	27.5	4	2*	2
	12D10D6S47I	4	351	479	4	363	27.5	2	2*	1
	12D10D4S47	4	351	479	2	671	25.3	5	4*	3
	12D10D4S47I	4	351	479	4	671	25.3	3	2*	3
	12D13D4S35	4	336	482	2	671	27	6	5*	5
	12D13D4S35I	4	336	482	4	671	27	5	5*	3
	12D10D4S35	4	351	479	2	671	27	4	5*	3
	12D10D4S35I	4	351	479	4	671	27	4	4*	3
Masamoto et al. [19]	8D10D6S70	3	379	523	2	392	27.1	1	1*	1
	8D10D6S70T	3	379	523	3	392	27.1	1	1*	1
	8D13D6S47	3	336	482	2	392	27.5	4	3*	3
	8D13D6S47T	3	336	482	3	392	27.5	3	2*	3
	8D10D6S47	3	379	523	2	392	27.5	3	2*	2
	8D10D6S47T	3	379	523	3	392	27.5	3	2*	1
	8D10D4S47	3	379	523	2	671	25.3	4	3*	3
	8D10D4S47T	3	379	523	3	671	25.3	3	2*	3
	8D13D4S35	3	336	482	2	671	27	6	5*	5
	8D13D4S35T	3	336	482	3	671	27	6	5*	3
	8D10D4S35	3	379	523	2	671	27	5	4*	3
	8D10D4S35T	3	379	523	3	671	27	4	4*	3
Kikukawa et al. [18]	8D13LD6S70	3	336	481	2	761	68.8	3	2*	2
	8D13LD6S70T	3	336	481	3	761	68.8	2	2*	1
	8D13LD6S47	3	336	481	2	761	68.8	4	3*	3
	8D13LD6S47T	3	336	481	3	761	68.8	3	3*	3
	8D13LD4S70	3	336	481	2	704	68.8	2	3*	2
	8D13LD4S70T	3	336	481	3	704	68.8	3	2*	3
	8D13LD4S47	3	336	481	2	704	70	4	5*	3
	8D13LD4S47T	3	336	481	3	704	70	4	4*	3

* Estimate based on Dhakal and Maekawa [6].

5. Model results for buckling of group bars

Several tests have been carried out to evaluate global and local buckling for columns with concentric axial load (e.g., [17–20]). The relevant material data and the lower observed buckling mode are shown in Table 2. The columns had an square section of 150 mm side with a core confined dimension estimated as $l = 130$ mm and a total length of $L = 530$ mm. The spacing of the stirrups ranged from $1.5d_b$ to $11d_b$, with most test in the range $4d_b$ to $6d_b$. The rebar yield stress for the specimens consid-

ered for comparison ranged from 336 to 761 MPa, whereas the concrete strength ranged from 22 to 70 MPa for a total of 61 tests. The material information is based on σ_y and σ_m, as well as the stress–strain response in tension for most cases, which are available in the literature. Few cases presented incomplete information, for which common parameter values were selected. The identification of the tests is as follows: $(n_1^o)D(n_2^o)D(n_3^o)S(n_4^o)$, where (n_1^o) represents the total amount of longitudinal rebar, (n_2^o) the diameter of longitudinal reinforcement, (n_3^o) diameter of stirrups, and (n_4^o) the separation of transverse reinforcement. The ending identification *l* or *T* reveals the presence of stirrup bars in intermediate bars in the case of 8 and longitudinal reinforcing bars 12, respectively. The high steel reinforcement (D13H-1) was not considered in the analysis, given the large difference observed for both models (13 cases).

A comparison between the buckling mode obtained with the proposed model for global buckling (Model), the model results by Dhakal and Maekawa (DM) and experimental results [17–20] is made. The results obtained for the models are shown in Table 2 and in Fig. 13a. Fig. 13a shows the correlation between the observed and predicted buckling mode for all cases. Perfect correlation would results in a diagonal representation. The numbers within the circles (and size – the bigger the size, the larger number of cases) correspond to the number of occurrence cases. The error values between the experimental observation and the buckling modes obtained with the model are shown in Fig. 13b. The error, in this case, is calculated as $Error_{Mode} = Mode_{Model} - Mode_{Test}$. The model yields global buckling modes lower than those observed experimentally with slightly higher errors (avg = −0.59, std = 0.88) than those obtained by applying the methodology by Dhakal and Maekawa (see Table 2), which gives an average error of -0.26 and standard deviation of 0.73. Most cases show an error of 0 or −1, indicating that the model fails to predict the number of stirrups within the buckled shape commonly in 0 or 1 (less than observed) unit. Although the differences, the model described in this study also allows defining the overall stress versus strain curve for the buckled bars which can be used in sectional or elements, such as columns or walls, nonlinear analysis.

Fig. 14 shows the overall response of column specimen 4D16HD6S35 (Fig. 14a) tested by Kato et al. [17], and specimens 12D10D6S47 (Fig. 14b) and 12D10D6S47I (Fig. 14c) tested by Ooya and Kato [20]. All columns are 150 by 150 mm on side and are reinforced with either 4ϕ16 mm high strength longitudinal bars (4D16HD6S35) or 12ϕ10 mm normal strength longitudinal bars and with ϕ6 mm stirrups at either 35 mm (4D16HD6S35) or 47 mm on center surrounding longitudinal bars (see Table 2). Specimen 12D10D6S47I presented additional transversal reinforcement tying all longitudinal bars. In order to determine the contribution of the longitudinal reinforcement to the overall response other identical columns were tested under the same conditions and configurations, except for the amount of longitudinal reinforcement. Specimens 4D16HD6S35 and 12D10D6S47 were compared with specimens with 4ϕ4 mm bars, whereas specimen 12D10D6S47I was compared with a specimen with 12ϕ4 mm bars in order to provide the same amount of transversal reinforcement, reducing the amount longitudinal reinforcement from about 4% to 0.2% in the first two cases, and reducing it to only 0.7% in the latest case. Although, the latest case correspond to a no significant reinforcement reduction, the response of a column with ϕ 4 mm results in a more pronounce degradation due to buckling given the larger stirrup versus longitudinal bar-diameter ratio. The longitudinal reinforcement contribution was determined by subtraction between the force applied to column under analysis with the force applied to the column with reduced longitudinal reinforcement. For comparison purposes the overall response has been corrected to the damaged length, determined by visual inspection, in order to compare with the model results. The strain within the damage length was determined as the displacement in the measurement length subtracted by the displacement determined with strain gauges outside the damaged length [17,20]. All test results indicate that the longitudinal bar buckles over 4 stirrups, i.e., $L/s = 4$ for specimen 4D16HD6S35, $L/s = 4$ for specimen 12D10D6S47 and $L/s = 2$ for specimen 12D10D6S47I. The model response is shown for cases with different buckling critical length (e.g., $L/s = 1$, 3, 4, 6), where $L/s = 3$ (specimen 4D16HD6S35), $L/s = 2$ (specimen 12D10D6S47) and $L/s = 1$ (specimen 12D10D6S47I) correspond to the case with the smallest peak capacity for each specimen, and therefore are selected as the characteristic lengths. Even though, those differ with the experimental observations, the overall stress versus strain response is quite similar to the experimental curve, except for the initial stage (before peak). It is important to indicate that other failure modes present strength that could be up to 30% higher than the one for the selected mode. The peak stress values for the selected model are about 10% lower than the experimental values, with a strain at the peak stress well represented by the model. Post-peak slope is important since it might be associated to overall degradation, which is associated to localization of damage as it has been seen in past earthquake [16]. The post-peak slope is also well capture with the model, with the largest difference observed for specimen 4D16HD6S35. In that case, the selected curve by the model presents a peak capacity just 3% lower than the next bucking length mode ($L/s = 4$), indicating that small changes in material properties or column geometry might easily change the selected curve to such case, which shows an improved post-peak response.

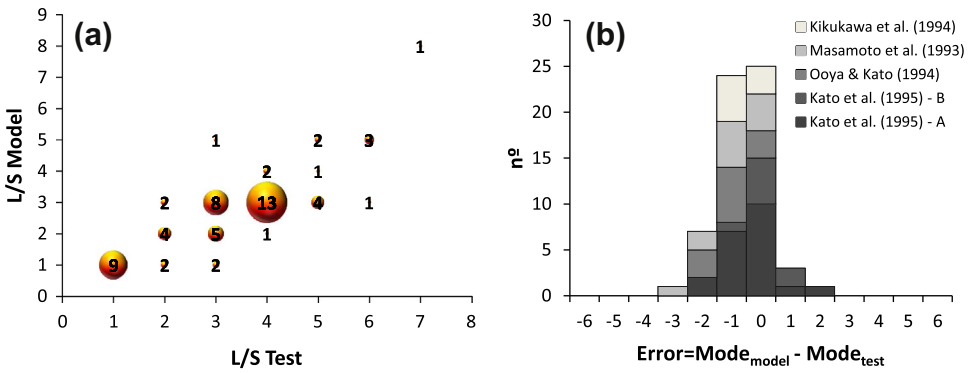

Fig. 13. Model buckling mode predictions – (a) L/s test versus L/s model, and (b) error estimate.

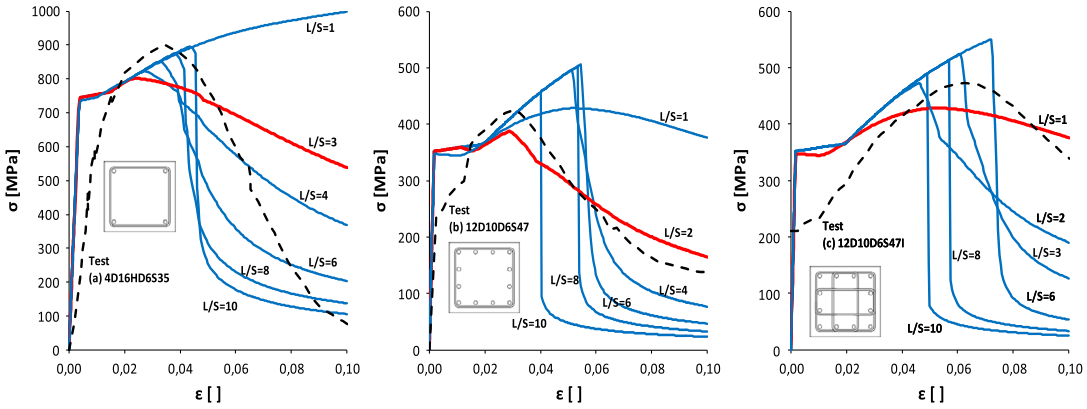

Fig. 14. Stress versus strain response – (a) 4D16HD6S35 [17], (b) 12D10D6S47 [20], and (c) 12D10D6S47I [20].

6. Summary and conclusions

The objective of this study is to represent the behavior of the longitudinal reinforcement in monotonic compression buckling considering the instability of the bar at a length that exceeds the distance between the stirrups and introducing the effect of transverse reinforcement in the analysis. For these purposes the model by Massone and Moroder [2] for local buckling of reinforcement, based on 4 plastic hinges, is adjusted to introduce the forces associated with transverse reinforcement within the buckling length and the effect of concrete expansion. Forces generated on stirrups beyond the action of the concrete expansion are balanced with the internal moment in the buckled bar.

For the analysis of group bar buckling in an element, an average behavior of the group bar is established based on equilibrium that includes all the stirrups acting at a certain height of the bar with identical longitudinal elongation and with all longitudinal bars under the same axial force (same bar diameter is considered), regardless of their location in the element cross section. This can be justified because the experimental evidence shows that differences between the buckling mode of bars directly constrained by a stirrups and unconstrained bars present is small, usually not exceeding the stirrup spacing. The selection criterion was taken as the buckling mode that yields the lowest maximum stress.

In terms of the buckling mode obtained with the model, expressing it in the amount of stirrup spacing L/s, the results are relatively good yielding an error comparable to the model by Dhakal and Maekawa [6], with an average error of −0.59 (about half a stirrup spacing) which is a good value, considering that the test database used has buckling modes ranging from 1 to 7. The methodology used for determining the buckling mode involves generating curves for several possible cases, thus, alternatively, the formulation by Dhakal and Maekawa could be used to select the buckling mode. The model described in this study, differently than most previous works, besides of predicting the buckling mode, provides the stress–strain curve for the buckled bars (σ–ε) which can be used in sectional or element analysis. Analysis of three column specimens from the literature indicates that even though the buckling mode might not be perfectly captured, the overall stress versus strain response can be obtained with a reasonable accuracy. Peak stress is obtained with an error about 10% compared to the test result for a strain well represented by the model. The post-peak slope also gives a good estimate for the degradation stage.

Acknowledgements

This work was partially financially supported by Chile's National Commission on Scientific and Technological Research (CONICYT) for the project Fondecyt 2008, Initiation into Research Funding Competition, under Grant No. 11080010.

References

[1] Papia M, Russo G, Zingone G. Instability of longitudinal bars in RC columns. J Struct Eng 1988;114(2):445–61.
[2] Massone L, Moroder D. Buckling modeling of reinforcing bars with imperfections. Eng Struct 2009;31(3):758–67.
[3] Bresler B, Gilbert P. Tie requirements for reinforced concrete columns. ACI J Proc 1961;58(26):555–69.
[4] Scribner C. Reinforcement buckling in reinforced concrete. ACI J Proc 1986;83(6):966–73.
[5] Russo G. A buckling model for reinforcing bars. Int J Mech Sci 1988;30(1):3–11.
[6] Dhakal R, Maekawa K. Reinforcement stability and fracture of cover concrete in reinforced concrete members. J Struct Eng 2002;128(10):1253–62.
[7] Lacaze C. Modeling and study of buckling effect in low cycle fatigue in longitudinal reinforcement of RC structures. Civil Engineering Thesis. University of Chile; 2009. p. 94 [in Spanish].
[8] Mander JB, Priestley MJN, Park R. Seismic design of bridge piers. Department of Civil Engineering, University of Canterbury. Report 84–2. 1984. p. 483.
[9] Dodd LL, Restrepo-Posada JI. Model for predicting cyclic behavior of reinforcing steel. J Struct Eng 1995;121(3):433–45.
[10] Pantazopoulou S. Detailing for reinforcement stability in RC members. J Struct Eng 1998;124(6):623–32.
[11] Menegotto M, Pinto PE. Method of analysis for cyclically loaded reinforced concrete plane frames including changes in geometry and non-elastic behavior of elements under combined normal force and bending. In: Proceedings, IABSE symposium; 1973.
[12] Mander J, Priestley M, Park R. Theoretical stress–strain model for confined concrete. J Struct Eng 1988;114(8):1804–26.
[13] Bayrak O, Sheikh S. Plastic hinge analysis. J Struct Eng 2001;127(9):1092–100.
[14] Sheikh S, Uzumeri S. Analytical model for concrete confinement in tied columns. J Struct Div 1980;108(12):2703–22.
[15] Massone LM. Fundamental principles of the reinforced concrete design code changes in Chile following the Mw8.8 earthquake in 2010. Eng Struct 2013;56:1335–45.
[16] Wallace JW, Massone LM, Bonelli P, Dragovich J, Lagos R, Lüders C, Moehle J. Damage and implications for seismic design of RC structural wall buildings. Earthquake Spectra 2012;28(S1):S281–99.
[17] Kato D, Kanaya J, Wakatsuki J. Buckling strains of main bars in reinforced concrete members. In: Proc., 5th East Asia and Pacific Conf. in structural engineering and construction EASEC-5. Gold Coast, Australia; 1995. p. 699–704.
[18] Kikukawa T, Ooya H, Kato D, Wakatsuki K. Buckling behaviors of intermediate steel bars in R/C columns. In: Summaries of technical papers of Annual Meeting Architectural Institute of Japan. Structures II; 1994. p. 353–356 [in Japanese].
[19] Masamoto K, Wakatsuki K, Ooya H, Kato D. Buckling behaviors of steel bars in R/C columns. In: Summaries of technical papers of Annual Meeting Architectural Institute of Japan. Structures II 1993, 787–792 [in Japanese].
[20] Ooya H, Kato D. Experimental study on buckling behavior of intermediate longitudinal bars in R/C members. Trans Jpn Concr Inst 1994;16:365–72.